Technical Report

Technology Development for Investigation of Phase Separation Structure of Polymer Alloys Using Scanning Transmission X-ray Microscopy

Sakura ORIGUCHI* Takayuki HARANO
Hiroaki OHARA Shinichiro SAKURAI

Abstract

In general, the mechanical and thermal properties of a polymer alloy composed of two or more polymers with contradictory properties are strongly related to its phase separation structure. In this paper, we reported the development for analytical techniques of phase separation structure of polymer alloys using scanning transmission x-ray microscopy (STXM) to visualize the chemical structure with submicron-scaled spatial resolution. In the case of the phase separation structure of polymer alloys consisting of phenoxy resin/nylon 12 with two compatibilizers, the distribution of compatibilizers was observed to change in a manner that depended on the type and amount of compatibilizer. Therefore, the desired mechanical properties can be achieved by controlling the morphology of the polymer alloy through the use of a compatibilizer, and that STXM is a suitable technique for investigating the relationship of phase separation structure changes and their properties in polymer alloys.

1. Introduction

With the progression of multi-functional and high-performance properties required for polymer materials in recent years, research has been actively conducted on polymer alloy technology that develops polymer materials having the characteristics of multi-component resins, which combines resins with contradictory properties. Examples of high performance achieved through polymer alloying include improving impact resistance by adding elastic acrylonitrile butadiene styrene (ABS) copolymer to hard and brittle polystyrene and imparting chemical resistance to highly heat-resistant polycarbonate by alloying it with polyethylene terephthalate.[1, 2] In such polymer alloys, each component resin is insoluble, but forms a phase separation, typically a sea-island structure. It is possible to change the phase separation structure by changing the chemical structure and molecular weight of the resins and by changing preparation conditions such as kneading temperature and shearing force. The use of additives such as compatibilizers that reduce the interfacial tension between the resins is also effective.[3]

The properties of polymer alloys depend on the phase separation structure. In order to obtain the desired physical properties, it is important to clarify the mechanism of phase separation structure formation and develop a method to control it. To this end, development is conducted not only on visualization technology to observe the phase separation structure correctly, but also on analytical techniques to investigate the miscibility state of the resins and the spatial distribution of the additives. Scanning electron microscopy (SEM) is widely used as a simple method to observe the phase separation structure. It is also effective for observing the fracture surface of polymer alloys because of its deep focal depth and its ability to acquire surface roughness information. However, its low spatial resolution and contrast make it difficult to obtain accurate information on the phase separation structure on the submicron scale. Many methods have been studied to combine transmission electron microscopy (TEM) with electron staining of resins with stains such as osmium tetroxide and ruthenium tetroxide. These methods can visualize fine-phase separation structures on the nanoscale. However,

* Basic Technology Integration Center, Research & Development Div., Nippon Steel Chemical & Material Co., Ltd.
1 Tsukiji, Kisarazu City, Chiba Pref. 292-0835

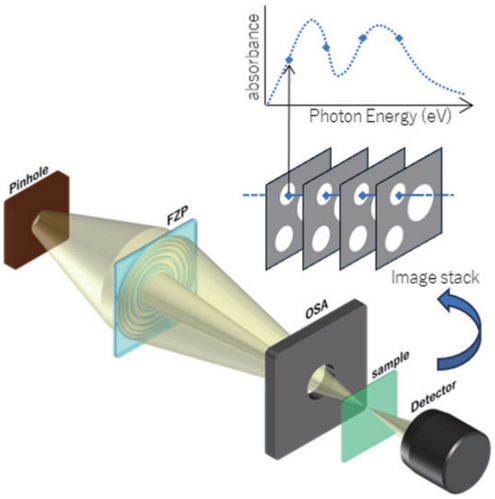

Fig. 1 Schematic diagram of STXM

the electron stains react chemically with certain functional groups of the resins and make it difficult to evaluate the functional groups of the respective phases quantitatively. In addition, artifacts may occur because the stains are localized at the phase separation interface and because electron beams easily damage resins composed of light elements. Atomic force microscopy (AFM) can obtain the contrast that reflects differences in mechanical properties, such as viscoelasticity between the resins, and has a high spatial resolution to visualize the phase separation structure. However, as with a TEM, AFM cannot clarify the spatial distribution of chemical structures.

Thereupon, Nippon Steel Chemical & Material Co., Ltd. has focused on the scanning transmission X-ray microscope (STXM), which has been developed recently and enables chemical state analysis of microscopic regions (**Fig. 1**). STXM is a technique to map X-ray absorption spectra with a spatial resolution of approximately 50 nm by two-dimensionally scanning a thin sample with synchrotron radiation X-rays focused to a submicron size with a Fresnel zone plate (FZP) and by scanning the X-ray wavelength (photon energy).[4, 5] By mapping the absorption intensity while changing the photon energy, it is also possible to obtain an image stack that combines the spatial distribution and the spectral data of the respective pixels. Since STXM uses soft X-ray synchrotron radiation, it can identify the chemical bonds of light elements (C, N, O).[4, 5] In addition, X-rays are suitable as an analysis method for polymer materials because of less damage to samples than electron beams.

In this paper, we describe the study for analysis of the phase separation of polymer alloys[6] with their adhesive strength improved by the addition of compatibilizers by using STXM at a synchrotron radiation facility in addition to conventional scanning electron microscope-energy dispersive X-ray spectroscopy (SEM-EDS), AFM, and scanning transmission electron microscopy (STEM).[7]

2. Experiments

2.1 Preparation of polymer alloys

Five samples were prepared by adding two types of compatibilizers I and II at 5 wt% and 10wt%, respectively, to polymer alloys of phenoxy resin and nylon 12 (**Table 1**). **Figure 2** shows the chemical structures of phenoxy resin, nylon 12, and compatibilizers I and II. The weight-average molecular weight (Mw) of compatibilizers I and II is 4 000 and 115 000, respectively, and their acid values are 54 and 250 mgKOH/g, respectively. The resins and compatibilizers were kneaded in a twin-screw extruder and formed into pellets.[6]

Table 1 Composition of each sample

(mass%)

Sample	Phenoxy Resin (mass%)	Nylon12 (mass%)	Compatibilizer (mass%)	
			I	II
1	50.0	50.0	–	–
2	47.5	47.5	5.0	–
3	45.0	45.0	10.0	–
4	47.5	47.5	–	5.0
5	45.0	45.0	–	10.0

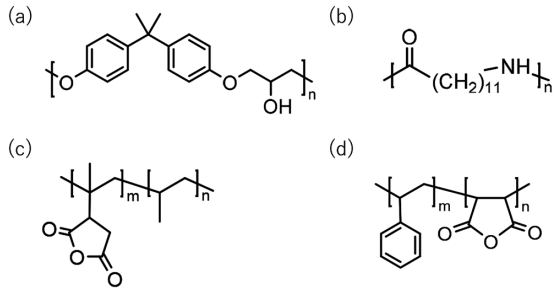

Fig. 2 Chemical structures of (a) Phenoxy resin, (b) Nylon12, and compatibilizers (c) (I) and (d) (II)

2.2 Preparation of measurement samples

Samples for SEM-EDS were embedded in epoxy resin, mechanically polished to expose the cross-section, and osmium deposited to provide electrical conductivity. Sections 70 nm in thickness for AFM and STEM were prepared using an ultramicrotome. Sections for STEM were collected on a TEM grid and electron stained with ruthenium tetroxide for 2 h. Each sample was sliced into 100 nm thick sections using an ultramicrotome and collected on a TEM grid. Pellets of samples 1 to 5 were used for SEM-EDS and STXM. Reference samples 3, prepared by melt kneading, were used for AFM and STEM.

2.3 Measurement methods

SEM backscattered electron images were observed at an accelerating voltage of 5 kV. AFM images were measured in the tapping mode to obtain height and phase images. Bright-field STEM images were obtained at an accelerating voltage of 30 kV for STEM observation. STXM was performed using a compact STXM (cSTXM) instrument at the beamline BL-19A of the Photon Factory at the High Energy Accelerator Research Organization (KEK).[8] In this study, X-ray absorption near edge structure (XANES) spectra were acquired around the energy (C K-edge) at which the 1s orbital electrons of the carbon atoms at each sample position are excited and image stack data is collected. XANES spectra for each compatibilizer were observed using 100 nm thick sections.

2.4 STXM data analysis method

The STXM data was analyzed using the analysis software aXis2000.[9] STXM spectra were extracted by encircling a given region from the image stack data. X-ray absorption images were acquired at photon energies corresponding to the chemical bond of in-

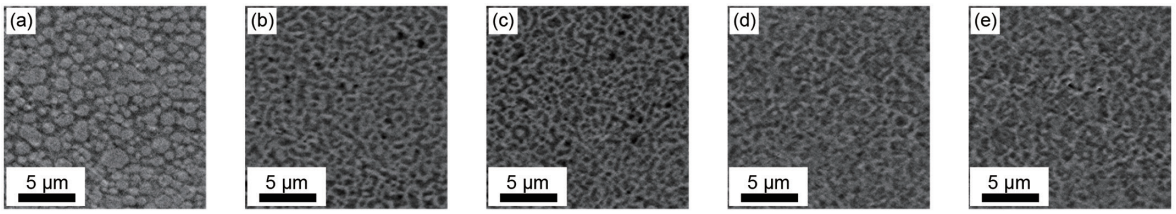

Fig. 3 SEM backscattered electron images of sample 1–5
(a) Sample 1, (b) Sample 2, (c) Sample 3, (d) Sample 4, (e) Sample 5

terest. The image stack spectrum data was analyzed using the spectra of phenoxy resin and nylon 12 in compatibilizer-free sample 1. The component distributions of phenoxy resin and nylon 12 were consequently obtained. The regions corresponding to phenoxy resin and nylon 12 are shown in purple and green, respectively.

3. Results and Discussion

SEM observations were performed to visualize the phase separation structure. **Figure 3** shows the SEM backscattered electron images of samples 1 to 5. The backscattered electron images were observed at low accelerating voltage and low illumination current to avoid electron beam damage. They were noisy but enabled the visualization of the phase separation structure. By nitrogen element (N) mapping using energy dispersive X-ray spectroscopy (EDS) for the sea-island structure of sample 1, N were detected in the sea domains. Of the components comprising the polymer alloy, only nylon 12 contains N. It is thus considered that the dark regions and bright regions in the backscattered electron images are nylon 12 and phenoxy resin, respectively. In compatibilizer-containing samples 2 to 5, the phase separation structure was observed to be refined. This refinement is generally considered to be the effect of surface tension reduction by a compatibilizer. However, it could not be judged whether the sea-island structure was refined in the original state or whether it was refined into a different phase separation structure. No dramatic change in the phase separation structure was observed even when the compatibilizer content was increased from 5 wt% to 10 wt%. Compatibilizers of different chemical structures were added to samples 2 and 3 and samples 4 and 5, respectively, but no clear difference in the phase separation structure was observed between these samples. Sample 3 was electron stained with ruthenium tetroxide and observed by STEM. The contrast of each phase was enhanced by electron staining, but the electron beam damage was so large that clear images could not be observed even when the magnification was increased.

AFM observation was performed to examine the phase separation structure in detail at a higher magnification than that of SEM and STEM. **Figure 4** shows the AFM height and phase images of sample 3, which was sectioned with an ultramicrotome. The height image shows surface irregularities, and the phase image shows the difference in the elastic modulus. AFM helped to visualize the phase separation structure. However, the contrast difference between the sea and island domains was small because the elastic modulus difference between the phenoxy resin and nylon 12 is small. The sea domains were very smooth. Small irregularities on the submicron scale were partially observed, but it is unclear whether they are due to phase separation or microtome cutting damage. Microscopic irregularities on the scale of several nanometers were observed inside the islands. The difference in shape makes it possible to distinguish the sea and islands. Clear sea-island interfaces were visible. Characteristic interface structures that would indicate the effect of a compatibilizer (for example, an interface structure where the elastic modulus changes gradually) were not observed. In addition, because chemical structural information cannot be observed with AFM, it is difficult to identify each phase in the phase separation of resins with small differences in the elastic modulus as in this study.

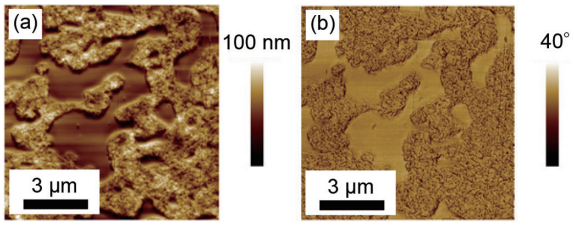

Fig. 4 AFM image (scan size: 10 μm × 10 μm) of sample 3
(a) Height sensor image, (b) Phase image

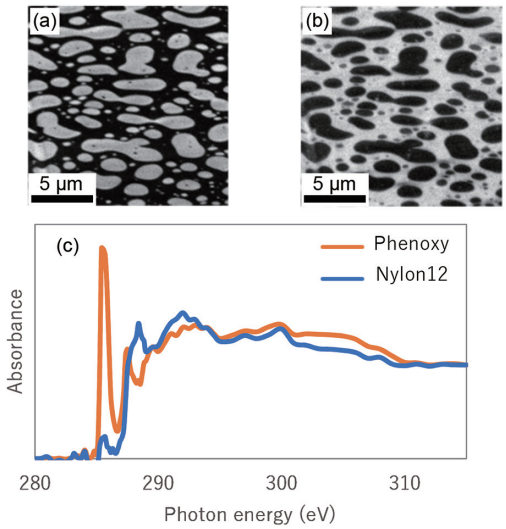

Fig. 5 X-ray absorption images at E = (a) 285.4 eV, (b) 288.4 eV for sample 1, (c) Average spectra of the lighter regions (phenoxy resin) and darker regions (nylon12) in Fig. 5 (a)

The X-ray absorption images of compatibilizer-free sample 1 at E=285.4 eV and E=288.4 eV are shown in **Figs. 5** (a) and 5 (b), respectively. The average C K-edge spectra extracted from the sea and island domains in the X-ray absorption images are shown in Fig. 5 (c). The X-ray absorption at E=285.4 eV corresponds to the 1s→π* excitation of the C=C bond and indicates the presence of phenoxy resin with an aromatic ring based on its chemical structure. The X-ray absorption at E=288.4 eV corresponds to the 1s→π* excitation of the carbonyl carbon of the amide bond and is a peak characteristic of nylon 12. The contrast of the X-ray absorption im-

ages reflects the absorption intensity of the X-rays. In the case of resins, this contrast difference is determined by the sample thickness and the chemical bond quantity. As the samples are sections of uniform thickness prepared with an ultramicrotome, the contrast of the X-ray absorption images is considered to indicate the chemical bond quantity. From the discussion, it was found that the bright island domains in Fig. 5(a) correspond to phenoxy resin because of the strong absorption intensity derived from the C=C bonds and that the dark sea domains correspond to nylon 12 because of the strong absorption intensity derived from the amide bonds. Note that the X-ray absorption image of Fig. 5(b) is mapped by the energy derived from the reversed contrast from Fig. 5(a) because it was mapped using the energy derived from the amide bonds specific to nylon 12.

In STXM X-ray absorption images (image size: 15×15 μm, 1 pixel is 50×50 nm), island domains on the micron to submicron scale were observed more clearly than in SEM images. In addition, the phenoxy resin domains in the island domains, which could not be confirmed by SEM due to noise, were observed in the island domains in the STXM X-ray absorption images. This observation is thought to be due to the fact that X-rays cause little damage to the sample, so a spectrum with a sufficiently high S/N ratio could be obtained. Also, because the sections are thin, in-depth information is not included.

We investigated whether the effect of the compatibilizer on the phase separation structure and its distribution state could be analyzed by STXM. **Figure 6** shows the X-ray absorption images of the respective samples at 285.4 eV. The phase separation size of compatibilizer-containing samples 2 to 5 was clearly smaller than that of compatibilizer-free sample 1. The data supports the SEM images. The sea-island structure observed in sample 1 was not observed in compatibilizer I-containing samples 2 and 3. Samples 2 and 3 instead showed the co-continuous structure. A comparison of samples 2 and 3 indicated that sample 2, containing 5 wt % of compatibilizer, formed a finer phase separation structure than sample 3. On the other hand, in compatibilizer II-containing samples 4 and 5, the islands were identified as nylon 12, and the sea was identified as phenoxy resin. The sea and island domains of the two samples are reversed with respect to sample 1. Samples 4 and 5 were confirmed to have no clear difference in the phase separation structure and to be uneven in the island size and distribution.

To investigate the interface state and the phase separation state in detail, we analyzed the component distribution of the high-magnification observation data (**Fig. 7**). In samples 2 to 5, no characteristic structural changes were observed in the interface state between phenoxy resin and nylon 12 due to the compatibilizer addition. On the other hand, when we looked inside the islands, we found that purple phenoxy resin components were dispersed in the green nylon 12 phase in compatibilizer II-containing samples 4 and 5. Qualitatively, more phenoxy resin was dispersed in the nylon 12 phase in sample 5 with a higher compatibilizer content than in sample 4. These results indicate that compatibilizers I and II do not have the effect of causing phenoxy resin and nylon 12 to invade each other at the phase separation interface to form a miscible intermediate phase, but that they are distributed at the interface like a general surfactant, reduce the interfacial tension, and finely disperse the phenoxy resin and nylon 12.

In order to evaluate the degree of invasion of the compatibilizer and the other resin into each phase, average spectra were extracted from the respective phases in Fig. 7, and the peak intensity fluctuations at 285.4 eV and 288.4 eV were analyzed. **Figure 8** shows the average spectra of the sea and island phases in reference sample 1 and compatibilizers I and II in the 283 to 290 eV region. Similar spectra were observed for compatibilizer I with nylon and for compatibilizer II with phenoxy. The strong peak of compatibilizer I around 288.4 eV is thought to be derived from the 1s→π* excitation of carbonyl carbon.

Figure 9(a) shows the spectra of samples 1 to 5 extracted from the purple regions of Fig. 7, which contain phenoxy resin as the main component. Comparing the peak intensity at 285.4 eV, samples 2 and 3 have lower peak intensity than sample 1. This result is considered to be due to the infiltration of compatibilizer I without an aromatic structure into the phenoxy resin phase. In addition, the compatibilizer content in the phenoxy resin phase tends to increase as the content of the added compatibilizer I increases. Sample 4 has al-

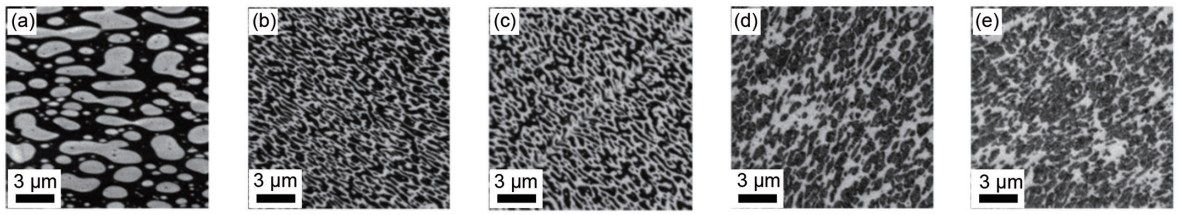

Fig. 6 X-ray absorption images of sample 1–5 at E=285.4 eV
(a) Sample 1, (b) Sample 2, (c) Sample 3, (d) Sample 4, (e) Sample 5

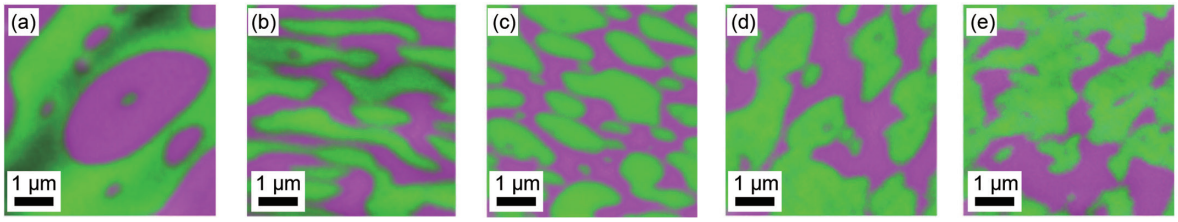

Fig. 7 Analysis image for each sample 1–5 at E=285.4 eV
(Purple and green regions correspond to areas where the phenoxy resin and nylon12 are the main components)
(a) Sample 1, (b) Sample 2, (c) Sample 3, (d) Sample 4, (e) Sample 5

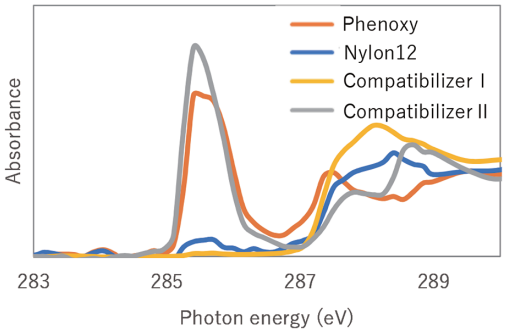

Fig. 8 Average spectra of the purple region (phenoxy resin phase) and the green region (nylon12 phase) in sample 1 (Fig. 7(a)), as well as compatibilizers I and II

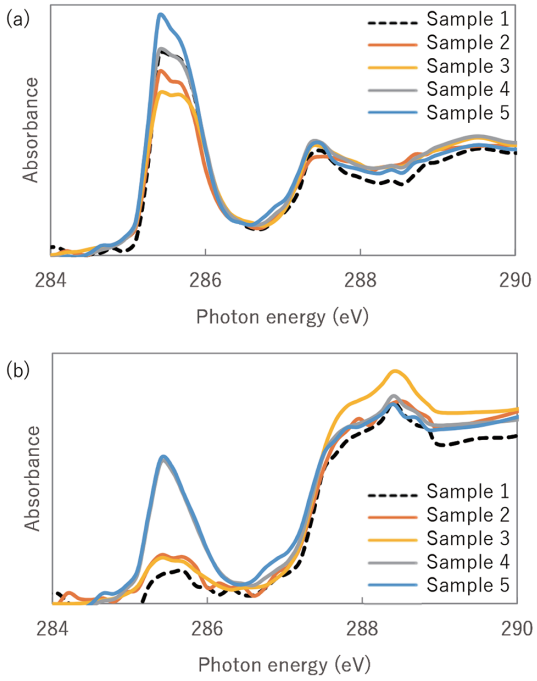

Fig. 9 C K-edge spectra of each phase in samples 1–5
(a) Purple region in Fig. 7 (phenoxy resin phase)
(b) Green region in Fig. 7 (nylon12 phase)

most the same peak intensity as sample 1, but sample 5 has higher peak intensity than sample 1. It was found that compatibilizer II does not infiltrate the phenoxy resin phase at 5 wt% or infiltrates the phenoxy resin phase in such a small amount that it cannot be detected. Clearly, it infiltrates into the phenoxy resin phase at 10 wt%. On the other hand, the peak intensity at 288.4 eV tends to be higher in samples 2 to 5 than in sample 1. In samples 2 and 3, the peak intensity decrease at 285.4 eV is linked with the peak intensity increase at 288.4 eV. This observation suggests the infiltration of the compatibilizer I into the phenoxy resin phase. In the case of sample 4, the peak intensity at 285.4 eV suggests that the compatibilizer II does not infiltrate into the phenoxy resin phase, so the increase in the peak intensity at 288.4 eV suggests the infiltration of nylon 12 components into the phenoxy resin phase.

Figure 9(b) shows the spectra of samples 1 to 5 extracted from the green domains in Fig. 7, which contain nylon 12 as the main component. Comparing the peak intensity at 285.4 eV, samples 2 and 3 have a slightly higher peak intensity than sample 1, suggesting the infiltration of the phenoxy resin into the nylon 12 phase. On the other hand, the peak intensity at around 288.4 eV is the highest for sample 3, and sample 2 is comparable to that of compatibilizer-free sample 1. This finding suggests that the compatibilizer I infiltrates more into the nylon phase as its content doubles. Samples 4 and 5 have a higher peak intensity at 285.4 eV than sample 1, suggesting the infiltration of the compatibilizer II or phenoxy resin into the nylon 12 phase. Comparing the peak intensity at 288.4 eV, samples 1, 4, and 5 have almost the same peak intensity. As the spectra of compatibilizer II and nylon 12 are similar, the peak intensity at 288.4 eV does not change despite the infiltration of compatibilizer II into the nylon 12 phase. The above discussion suggests the infiltration of not the phenoxy resin but the compatibilizer II into the nylon 12 phase. In addition, samples 4 and 5 have almost the same peak intensity, probably because the compatibilizer II preferentially infiltrates into the nylon 12 when 5 wt% is added, also in consideration of the result of Fig. 9(a) that the compatibilizer II when 10 wt% is added infiltrates into the phenoxy resin.

Most polymers are not miscible. However, in cases where two or more types of polymers are compatibilized, the chemical structures of their main chains and side chains are often similar. Apart from the chemical structure, the molecular weight has a strong influence. Polymers with smaller molecular weights more readily tend to be compatibilized with each other. In addition, for the polymer alloys in this study, it is postulated that the hydroxyl and carbonyl groups in the resin react with the maleic anhydride groups in the compatibilizer during melt kneading of the polymer alloy.[10] The higher the modification rate of the compatibilizer, the higher the reactivity between the resin and the compatibilizer, and therefore the higher the miscibility. The compatibilizer II has a higher modification rate than the compatibilizer I and is thus expected to have a higher miscibility.

Considering the above discussion, the phase separation structure and compatibilizer dispersion state are summarized in **Fig. 10** according to the STXM data. In samples 2 and 3, the compatibilizer I is distributed in the nylon 12 phase, probably because it has a chemical structure similar to that of nylon 12. On the other hand, the compatibilizer I is incorporated into the phenoxy resin phase probably because it has a low molecular weight and reacts with the phenoxy resin. Furthermore, the phenoxy resin-compatibilizer I reactant has a chemical structure similar to that of nylon 12 and is thus considered to invade the nylon 12 phase. This consideration does not contradict the STXM results. In samples 4 and 5, contrary to expectations, the compatibilizer II infiltrates into nylon 12 preferentially over phenoxy resin, which has a similar structure. This condition is probably related to the high molecular weight of the compatibilizer II and the high modification rate of maleic anhydride groups. However, this supposition cannot be explained by the results of this study. This difference in the infiltration degree of the compatibilizer is presumed to affect the formation of the phase separation structure. The consideration that nylon 12 infiltrates a little into phenoxy resin is reasonable because nylon 12 and the compatibilizer are miscible and then react. Sample 4 with compatibilizer II has a more heterogeneous morphology than sample 2 with compatibilizer I (Fig. 7), and the phenoxy resin and nylon 12 are partly mixed, suggesting that some of the reactants are infiltrated into the phenoxy resin phase.

4. Conclusions

In this study, we clarify the distribution of compatibilizers using STXM, which provides submicron-scale chemical structure infor-

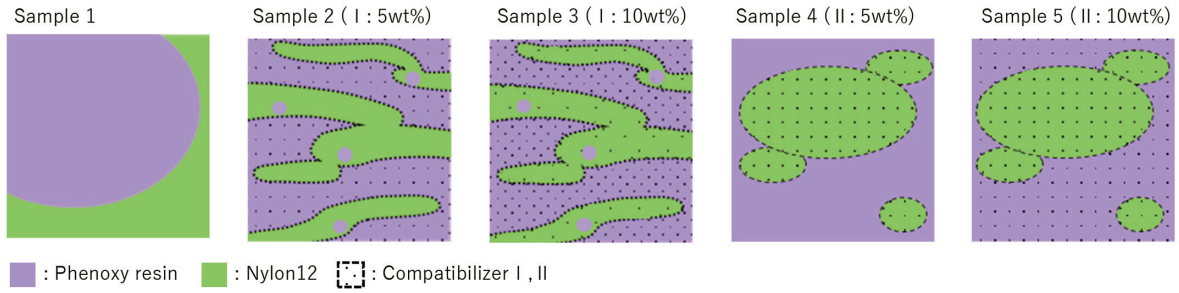

Fig. 10 Schematic diagram of the effect of compatibilizer I and II on the phase separation structure of phenoxy resin and nylon12

mation and showed that STXM is an effective technique for analyzing the phase separation structure of polymer materials. In our previous polymer alloy studies, we understood the phenomenon of phase separation structures being refined by compatibilizers. However, the effect of the compatibilizer had many unclear points. According to the STXM results reported here, we were able to consider, albeit qualitatively, the relationships of the phase separation structure change with compatibilizer influence factors, such as the compatibilizer distribution state, chemical structure, molecular weight, reactive functional group modification rate, reactivity with resins, and change in interfacial energy between the resins. In the future, we will expand the phase separation structure evaluation using STXM to other polymer alloys to elucidate the mechanisms of phase separation and to identify factors related to material properties.

Acknowledgments

This study was conducted in collaboration with Professor Masao Kimura of the High Energy Accelerator Research Organization. We would like to express our sincere gratitude to him for his guidance and cooperation in measurements and data analysis.

References

1) Izawa, S.: J. Soc. Mat. Sci. 41 (465), 789 (1992)
2) Barlow, J.W. et al.: Polym. Eng. Sci. 21, 985 (1981)
3) Inoue, T.: Polymers. 45 (7), 447 (1996)
4) Kikuma, J.: J. Adhesion Soc. Jpn. 49 (11), 421 (2013)
5) Takeichi, Y.: Jpn. APPLIED PHYSICS. 89 (9), 509 (2020)
6) Japanese Patent Application Publication No.2023-174176. December 7, 2023
7) Harano, T. et al.: AIP Conf. Proc. 2990, 020013-1 (2023)
8) Hitchcock, A.P.: J. Electron Spectrosc. Relat. Phenom. 266 147360 (2023)
9) Takeichi, Y. et al.: Rev. Sci. Instrum. 87, 013704-1 (2016)
10) Nishio, T. et al.: KOBUNSHI RONBUNSHU. 47 (4), 331 (1990)

Sakura ORIGUCHI
Basic Technology Integration Center
Research & Development Div.
Nippon Steel Chemical & Material Co., Ltd.
1 Tsukiji, Kisarazu City, Chiba Pref. 292-0835

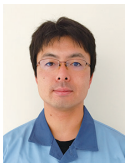

Hiroaki OHARA
Ph.D. in Engineering, Researcher
At the time: Basic Technology Integration Center
Research & Development Div.
Nippon Steel Chemical & Material Co., Ltd.

Takayuki HARANO
Ph.D. in Engineering, Researcher
At the time: Basic Technology Integration Center
Research & Development Div.
Nippon Steel Chemical & Material Co., Ltd.

Shinichiro SAKURAI
Ph.D. in Engineering, Group Leader
Basic Technology Integration Center
Research & Development Div.
Nippon Steel Chemical & Material Co., Ltd.